Journal of Materials Chemistry A

Accepted Manuscript

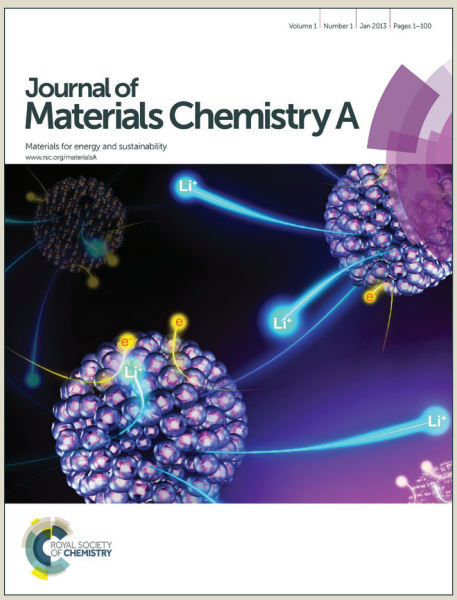

ROYAL SOCIETY OF CHEMISTRY

www.rsc.org/materialsA

Journal of Materials Chemistry A RSCPublishing

ARTICLE

Beyond the H_2/CO_2 upper bound: one-step crystallization and separation of nano-sized ZIF-11 by centrifugation and its application in mixed matrix membranes for H_2/CO_2 separation

Cite this: DOI: 10.1039/xoxxoooooox

Received ooth January 2012,
Accepted ooth January 2012

DOI: 10.1039/xoxxoooooox

www.rsc.org/

Javier Sánchez-Laínez,[1] Beatriz Zornoza,[1] Álvaro Mayoral,[2] Ángel Berenguer-Murcia,[3] Diego Cazorla-Amorós,[3] Carlos Téllez,[1] Joaquín Coronas[1,*]

The synthesis of nano-sized ZIF-11 with an average size of 36±6 nm is reported. This material has been named nano zeolitic imidazolate framework-11 (nZIF-11). It has the same chemical composition and thermal stability properties and analogous H_2 and CO_2 adsorption properties as the conventional microcrystalline ZIF-11 (i.e. 1.9±0.9 μm). nZIF-11 has been obtained following the centrifugation route, typically used for solid separation, as a fast new technique (pioneering for MOFs) for obtaining nanomaterials where the temperature, time and rotation speed can easily be controlled. Compared with traditional synthesis consisting of stirring + separation, the reaction time was lowered from several hours to a few minutes when using this centrifugation synthesis technique. Employing the same reaction time (2, 5 or 10 min), micro-sized ZIF-11 was obtained in the traditional synthesis while nano-scale ZIF-11 was achieved only by using centrifugation synthesis. The small particle size obtained for nZIF-11 allowed the use of the wet MOF sample as a colloidal suspension stable in chloroform. This helped to prepare mixed matrix membranes (MMMs) by direct addition of the membrane polymer (polyimide Matrimid®) to the colloidal suspension, avoiding particle agglomeration resulting from drying. The MMMs were tested in H_2/CO_2 separation, improving the pure polymer membrane performance, with permeation values of 95.9 Barrer of H_2 and a H_2/CO_2 separation selectivity of 4.4 at 35 ^{0}C. When measured at 200 ^{0}C, these values increased to 535 Barrer and 9.1.

Introduction

Zeolitic imidazolate frameworks (ZIFs) are a subfamily of metal-organic frameworks (MOFs) in which a metal cation of Zn^{2+} or Co^{2+} is linked to the nitrogen atoms of deprotonated imidazole molecules forming tetrahedral frameworks in zeolite-like topologies.[1] ZIFs constitute highly porous frameworks with extraordinarily high thermal and chemical stabilities. They have a great number of potential applications such as gas sorption,[2] gas separation,[3,4] drug delivery[5] and catalysis.[6,7] Due to its small pore size, ZIF-11 is one of the most promising ZIFs for gas separation. It forms a RHO type zeolitic structure were Zn^{2+} is the metal ion and benzimidazole (bIm) the organic linker.[8] The well-defined porous structure with large cavities of 14.6 Å connected through pore apertures of 3 Å, similar to the kinetic diameter of H_2 (2.9 Å), makes it ideal for hydrogen separation by the sieving process.[9] It has been estimated by molecular simulation that at room temperature ZIF-11 can achieve a H_2/CO_2 selectivity of 262 with a H_2 permeability of 5830 Barrer. It is thus a perfect candidate for pre-combustion capture.[10] However, its applications are still underdeveloped, mainly due to its micrometric size, i.e. to the lack of a synthesis method able to produce nano-sized ZIF-11.

MOF nanoparticles are of great interest in the engineering world due to their unique physical, chemical and optical properties and their high surface to volume ratio.[11] Many researchers have focused their efforts on reducing the crystal size to the nanoscale besides reducing the synthesis time through several methods beyond solvothermal synthesis,[12] including ultrasound bath,[13] microwave-assisted crystallization,[14] microemulsion,[15] microfluidics,[16] etc. However, precise control over the size and shape of MOFs still remains a challenge.[17] Some ZIFs have already been synthesized as nanoparticles, such as ZIF-7[18] or ZIF-8,[19] but this has not been achieved for ZIF-11 since this material was first obtained by Yaghi´s group.[9] A friendlier alternative to the common amide-based solvents such as N,N-dimethylformamide (DMF) and N,N-diethylformamide (DEF), difficult to remove from pores,[20] is the use of methanol. In this procedure, reported by Ming et. al.,[21] toluene is also used as a

structure director in the synthesis of ZIF-11, but still within the 1-4 µm size range.

During the synthesis of zeolites, which have a common topology with ZIFs, amorphous precursors can be obtained. These precursors show no crystallinity but present pore dimensions and topologies very close to zeolites, having similar properties.[22] Analogous structures can also be obtained in the synthesis of MOFs, as already reported for HKUST-1 or MIL-89.[23, 24]

In this work nano-sized ZIF-11 (nZIF-11) has been synthesized under centrifugal acceleration, showing similar physical and chemical properties to the microcrystalline ZIF-11. nZIF-11 has been integrated in commercial polyimide Matrimid® continuous phase, forming mixed matrix membranes (MMMs) able to enhance the performance of the pure polymer in the H_2/CO_2 separation process. The filler was used as a colloidal suspension, similarly to Chung et. al. procedure with nano-sized ZIF-7 and DMF.[25] Finally, this separation process is focused on H_2 purification and in particular to the so called precombustion CO_2 capture.

Experimental

Chemicals

Zinc acetate dihydrate ($Zn(CH_3COO)_2 \cdot 2H_2O$), benzimidazole (bIm, $C_7H_6N_2$, 98 %), ammonium hydroxide (NH_3, 28-30% aqueous solution), chloroform (anhydrous) and toluene (≥99.5%) were purchased from Sigma Aldrich. Methanol (HPLC grade) was purchased from Scharlau. Matrimid® 5218 was kindly supplied by Huntsman Advanced Materials.

Nano-sized ZIF-11 synthesis

0.24 g of bIm (2 mmol) was dissolved in 6.4 g of methanol (400 mmol), together with 9.2 g of toluene (100 mmol) and 2.4 g of ammonium hydroxide (40 mmol). 0.22 g of Zinc acetate dihydrate (1 mmol) was dissolved in 3.2 g of methanol (200 mmol). Both solutions were cooled separately to 18 ºC and then mixed in a centrifuge flask of 50 mL at 10000 rpm at that temperature. The centrifugation time varied between 1 and 30 min. Note that 1 min is the time needed to achieve such rotation speed. The solid collected was washed with methanol three times for the complete removal of toluene and dried at 100 ºC overnight for characterization purposes. The molar composition of the mixture was $Zn:bIm:NH_3:CH_3OH:toluene=1:2:40:300:100$.[21]

Micro-sized ZIF-11 synthesis

The same reactant amounts and steps as in the previous procedure were applied. However, instead of centrifuging, the mixture was stirred from a few minutes to 3 h at room temperature before collecting the solid by centrifugation at 10000 rpm and washing it.

MMM fabrication

When using the material as filler for MMMs, instead of being dried, the methanol-collected ZIF-11 nanoparticles were further washed with chloroform to avoid agglomeration. After the third centrifugation, the particles were re-suspended in chloroform prior to use. The suspension concentration was calculated for each membrane loading: 10, 15 and 25 wt%, and the corresponding amount of polyimide Matrimid® powder was added. The addition of polymer to the nZIF-11 dispersion was done in two stages while stirring and the resulting solution was further stirred overnight. The casting solution was three times stirred and sonicated alternatively for 90 min and cast into a petri dish at room temperature. The petri dishes were left covered overnight for slow evaporation of the solvent. After that, the membranes were peeled off from the petri dishes and treated in a vacuum oven at 180 ºC and 10 mbar for 24 h for complete removal of the remaining solvent.

Membrane thicknesses were tested by a Digimatic Micrometer (measurement range from 0 to 30 mm with an accuracy of ±1 µm). Several points (9) equally distributed on the membrane were measured per membrane and the arithmetic average was used for the membrane thickness. In this work, the MMMs obtained have a thickness of 87±12 µm. For permeation testing of the membranes, circular areas of 15.2 cm^2 were cut from the films.

Characterization of samples

Powder X-ray diffraction (XRD) spectra of nano-MOFs and MMMs were acquired using a D-Max Rigaku X-ray diffractometer with a copper anode and a graphite monochromator to select CuKα radiation (λ = 1.540 Å), taking data from 2θ=2.5º to 40º at a scan rate of 0.03 º/s. Thermogravimetric analyses (TGA) were carried out using a Mettler Toledo TGA/STDA 851e. Samples (10 mg) placed in 70 µL alumina pans were heated in an air flow from 25 to 900 ºC at a heating rate of 10 ºC/min. Scanning electron microscopy (SEM) images of MOFs and membranes were obtained using an Inspect F50 model scanning electron microscope (FEI), operated at 20 kV. Cross-sections of membranes were prepared by freeze-fracturing after immersion in liquid N_2 and subsequently coated with Pt. Transmission electron microscopy (TEM) images of the MOF were obtained using a FEI Tecnai F30 microscope, operated at 300 kV. The samples were prepared by dispersion of the powder in ethanol before placing a few drops of the suspension onto the copper carbon coated microgrid. Fourier transform infrared spectroscopy (FTIR) was performed on a Bruker Vertex 70 FTIR spectrometer equipped with a DTGS detector and a Golden Gate diamond ATR accessory. Powder samples were prepared by the KBr wafer technique and the measurements were done in a diffuse reflectance module. Both spectra were recorded by averaging 40 scans in the 4000-600 cm^{-1} wavenumber range at a resolution of 4 cm^{-1}. Particle size was obtained using ImageJ 1.49b software. At least 300 particles were counted for the nano-sized samples and 30 for the micro-sized, as particle density in SEM images is much lower. NMR Spectra were recorded in a Bruker Avance III WB400 spectrometer with 4 mm zirconia rotors spun at the magic angle in N_2 at 10 kHz. ^1H-^{13}C CP spectra were measured using a ^1H π/2 pulse length of 3.0 µs, with a contact time (ramp) of 3 ms, a spinal 64 proton decoupling sequence of 5.3 µs pulse length, and a recycle delay of 5 s. 3000 scans were acquired for each spectra.

High and low pressure adsorption analysis

High pressure hydrogen and carbon dioxide adsorption measurements were carried out in an automatic volumetric apparatus (Quantachrome iSorb HP1) to perform hydrogen isotherms up to 4 MPa and carbon dioxide isotherms up to 3.4 MPa. The manifold of

the apparatus was kept at 35 ^{0}C. In the case of hydrogen, the sample cell was refrigerated at the adsorption temperature (-196 ^{0}C) by means of a thermostated liquid nitrogen deposit which pumped the necessary amount of cryogenic liquid into a Dewar deposit to ensure a constant liquid nitrogen level and a stable sample temperature throughout the experiment. For the CO_2 experiments, a circulator bath set to 0 ^{0}C was employed. The manifold volume was calibrated with a standard volume, performing helium isotherms prior to each experiment. In order to ensure that the apparatus was leak-free, hydrogen leak tests were executed at 9 and 15 MPa for 28 h, the resulting leak rate being below 10^{-6} torr/(torr.s). The bulk gas amounts were calculated by the modified Benedict–Webb–Rubin equation of state,[26] and the cell volume was calculated taking into account the correction described in the literature.[27] Prior to the adsorption, the sample was degassed at 150 ^{0}C for 4 h under vacuum. After that, the sample was located in the sample holder, and then evacuated at 150 ^{0}C for 4 h under vacuum. Sample masses ranged between 0.5 and 1.0 g to ensure accurate measurements.

Carbon dioxide adsorption isotherms of ZIF-11 and nZIF-11 (synthesis of 5 min and 1 min) were also measured using a volumetric adsorption analyzer (Micromeritics ASAP 2020) at 0 ^{0}C up to 120 kPa after degassing at 200 ^{0}C for 8 h. In all cases, the hydrogen, carbon dioxide and helium gases used in the experiments were 99.9995% pure.

Gas separation analysis

Mixture permeability analyses were performed for polyimide based MMMs with nZIF-11 loadings of 10, 15 and 25 wt%, and ZIF-11 with 10 wt% loading for comparison. The membranes were introduced into a module consisting of two stainless steel pieces and a 316LSS macroporous disk support (from Mott Co.) with a 20 µm nominal pore size, gripped inside with silicone o-rings. The permeation module was placed in a UNE 200 Memmert oven to control the temperature of the experiments. Gas separation measurements were carried out by feeding a H_2/CO_2 equimolar mixture (25/25 cm^3(STP)/min) at 330 kPa to the feed side by means of two flow-mass controllers (Alicat Scientific, MC-100CCM-D), while the permeate side of the membrane was swept with a 1 cm^3(STP)/min mass-flow controller stream of Ar at 124 kPa (Alicat Scientific, MC-5CCM-D). Concentrations of H_2 and CO_2 in the outgoing streams were analyzed by an Agilent 3000A online gas microchromatograph equipped with a thermal conductivity detector. Permeability was calculated in Barrer (10^{-10} cm^3(STP)·cm/(cm^2·s·cmHg)) once the steady-state of the exit stream (for at least 3 h) was reached, and the separation selectivity was calculated as the ratio of permeabilities.

Colloidal suspension stability

A stability study was performed in order to prove the stability of the colloidal suspension and the need of keeping it wet to avoid agglomeration. Amounts (0.19 g) of wet and dry nZIF-11 were separately dispersed in chloroform (27.3 g). Both suspensions were left still for 20 days so as to observe changes in their homogeneity.

Results and discussion

nZIF-11 characterization

The synthesis method (traditional stirring + separation vs direct centrifugation) and the reaction time appear to be the critical variables in the formation of nZIF-11 or ZIF-11.

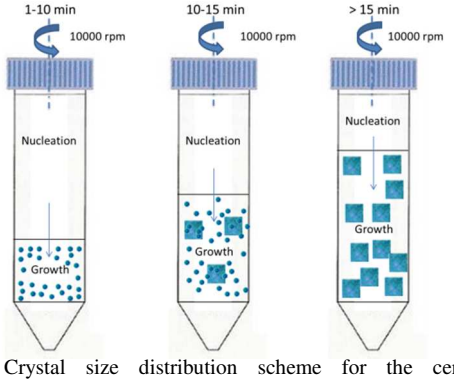

Figure 1. Crystal size distribution scheme for the centrifugation crystallization process at 18 ºC.

During synthesis by centrifugation two different zones may appear inside the centrifuge tube, a nucleation zone in the upper part (from which the centrifugal force removes nucleated particles) and a growth zone at the bottom using the settled nuclei (see Fig 1). For synthesis times lower than 10 min, ZIF-11 nanoparticles settled down from the nucleation to the growth zone were not able to grow because the process ended too early and remained nano-sized. For times between 10 and 15 min some of the crystals that settled down (the older crystals) had time to grow while others did not, thus a heterogeneous distribution of nano- and micro-sized crystals appeared. Eventually, for times higher than 15 min, the nucleation and growth were not separated, resulting in a micro-sized distribution.

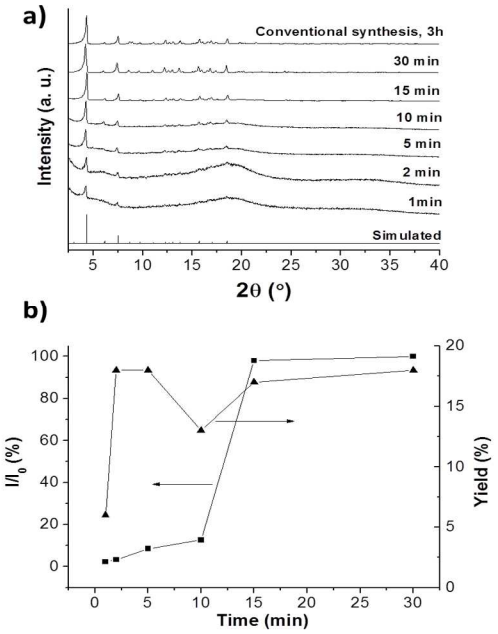

Figure 2. (a) XRD patterns of ZIF-11 samples synthesized at different reaction times and (b) evolution of crystallinity (calculated from main peak at 4.3º) and synthesis yield with time.

XRD spectra of ZIF-11 powder, synthesized at different times and by different methods (conventional stirring and centrifugation), are represented together with the simulated spectra of ZIF-11 in Fig. 2a. For 1 and 2 min an amorphous band for angles between 10 and 22^0 appears, showing that the material was not yet completely crystalline. All the spectra show the characteristic peaks of ZIF-11 at angles lower than 10^0, their width not matching the crystal nanosize when calculated with the Scherrer equation. The presence of few micrometric crystals of ZIF-11, evidenced in TEM images but not through SEM inspection (due probably to coating with nano-sized particles) must be responsible for these crystalline features. In fact, the evolution of the crystallinity with time is also shown in Fig. 2b, where the absolute intensity of the highest peak of ZIF-11 (2θ=4.3º) is represented. The plot shows very low values for times under 5 min, low values from 5 to 10 min, and a big increase at 15 min.

The results are consistent with the products obtained. Low intensities correspond to times when the nZIF-11 is predominant. At 15 min the first micrometric-sized crystals of ZIF-11 are obtained, and therefore the crystallinity of the mixture greatly increased. In any event, the relative crystallinity of about 8% reached after 5 min (2% after 1 min) would indicate a small amount of micro-sized particles, most of the material corresponding to nZIF-11. Fig. 2b also shows the nZIF-11 synthesis yield, calculated as the mol of MOF obtained per mol of metal cation used as reagent. The value is near 20% for all cases except for the 1 min sample, which is two-thirds lower.

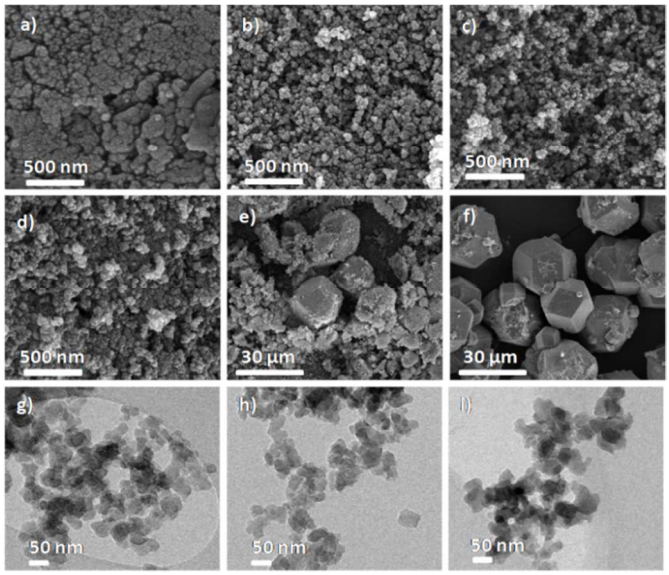

Figure 3. SEM images of samples synthesized by centrifugal acceleration at different reaction times: a) 1 min , b) 2 min, c) 5 min, d) 10 min, e) 15 min, and f) 30 min; TEM images at: g) 2 min, h) 5 min and i) 10 min. TEM image at 1 min can be seen in the SI (Fig. S1).

SEM images (Fig. 3a-f) reveal a non-defined particle shape for 1 min of reaction time. For 2 min the first nanoparticles appear, their shape similar to those of the samples of 5 and 10 min. At 15 min micro-sized crystals are evident and the nanoparticles finally disappear at 30 min. TEM images reveal a more accurate shape of the nanoparticles for times below 15 min (see Fig 3g-i). These nano-sized particles did not exhibit electron diffraction. We hypothesize that the critical energy dose reached by the nanoparticles would have been responsible for destroying the possible electron-diffraction pattern.[28] In agreement with the XRD patterns (shown in Fig 2a), the TEM images also show the presence of a small proportion of micro-sized crystals. These were covered by the nanometric particles that could not be appreciated in SEM images and have similar SAED features than micro-sized crystals. Fig S2 shows SAED patterns along [110] and [100] directions of ZIF-11 micro-sized particles which can be indexed to the *Im-3m* space group corresponding to the RHO type structure.

The corresponding normalized cumulative number of particles is represented in Fig. S3a as a function of particle size. From this plot, an average size for each sample was obtained at $N/N_T = 0.5$. The diameter increases from 36±6 nm for the 5 min sample to 17±2 µm corresponding to 30 min of synthesis time. In addition, the differential distribution was calculated (Fig. S3b), providing the predominant particle diameter (mode). The average and predominant sizes are shown in Table S1. The values are similar to the corresponding averages except for the 15 min sample, at which time both micro-and nano-sized crystals are depicted.

This one-step centrifugation process contrasts with the traditional synthesis, where crystals grow when stirred and are then collected by centrifugation. In this case, micro-sized crystals are obtained even for very low stirring times (see Fig. S4).

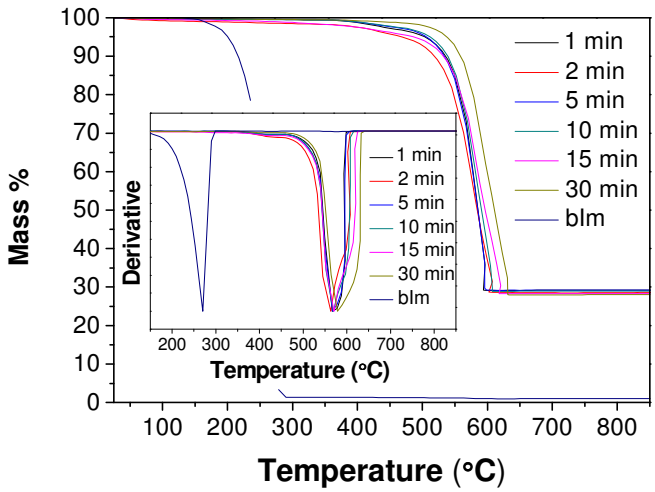

Figure 4. TGA and derivative curves (insert) in air of the samples synthesized at different reaction times. TGA of ligand bIm is shown for comparison.

The thermal stability of nZIF-11 in open air was measured by TGA (Fig 4). It can be seen how each synthesized sample has almost the same thermal stability, with an onset temperature over 400 ^{0}C, much higher than that of the organic ligand bIm (200^0C). This means that the nano-sized ZIF-11 is as stable as the micrometric ZIF-11, as both types of size are included among the different samples measured. This suggests the same nature of the chemical bond between ligand and metal in both the nano- and micro-sized materials. The residue weight remaining at the end of the analysis (≈25 wt% for all nano- and micro-sized samples) is due to the

oxidation of Zn metal to ZnO. Moreover, TGA also proves the need for three washes with methanol for the complete removal of toluene (used during the synthesis as a co-solvent and structuring agent) from the pores of ZIF-11 (Fig S5).

The FTIR spectra are explained in detail in the Supporting Information. The same bands for nZIF-11 and micro-sized ZIF-11 were found (Fig. S6) proving that both types of crystal have the same bond structure, consistent with the thermal stability shown by the TGA results.

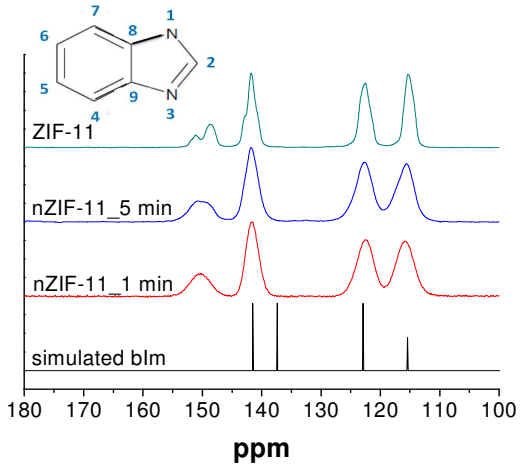

Figure 5. ^{13}C NMR spectra of nZIF-11, ZIF-11 and the organic ligand.

Fig. 5 shows the measured ^{13}C NMR spectra of micro- and nano-sized ZIF-11 (1 and 5 min), compared to the simulated spectrum of bIm. The characteristic bIm peaks at 122.9 (C5, C6) and 115.4 ppm (C4, C7) are slightly shifted to 122.5 and 115.9 ppm, respectively. However, the largest differences occur for the signals corresponding to the C8, C9 (137.9 ppm) and C2 (141.5 ppm), close to nitrogen atoms coordinated to the metallic clusters, displaced in ZIF-11 type materials to 141.8 and about 150 ppm (split into 148.6 and 151.1 for ZIF-11), respectively. These chemical shifts of ^{13}C signals are indicative of the presence of anionic [bIm^-], consistent with its deprotonation during the ZIF-11 formation.[32] Besides the splitting of the signal at about 150 ppm seen in the micro-sized ZIF-11 spectrum, slight differences of about 1 ppm between the micro- and nano-sized ZIF-11 peaks can be observed. In any event, the 5 min sample tends to be more similar to the micro-sized ZIF-11 than the 1 min sample. Like the previous characterizations, ^{13}C NMR suggests strong similarities in the chemical bond between both nano- and micro-sized samples, as well as subtle differences in the ZIF-11 ligand (bIm) coordination which may be due to both the lack of crystallinity and the higher external area (explained below) that nZIF-11 particles exhibit as compared to ZIF-11.

Gas adsorption measurements

Gas adsorption was measured for nZIF-11 to study its porosity. The compound was unable to adsorb N_2 at low relative pressures due to its narrow microporosity, proving that, as in the case of microcrystalline ZIF-11, the pore aperture is smaller than the N_2 molecule kinetic diameter (3.64 Å). Nevertheless, the nano-sized ZIF did show H_2 and CO_2 adsorption which indicates the presence of narrow microporosity as observed with ZIF-11[9].

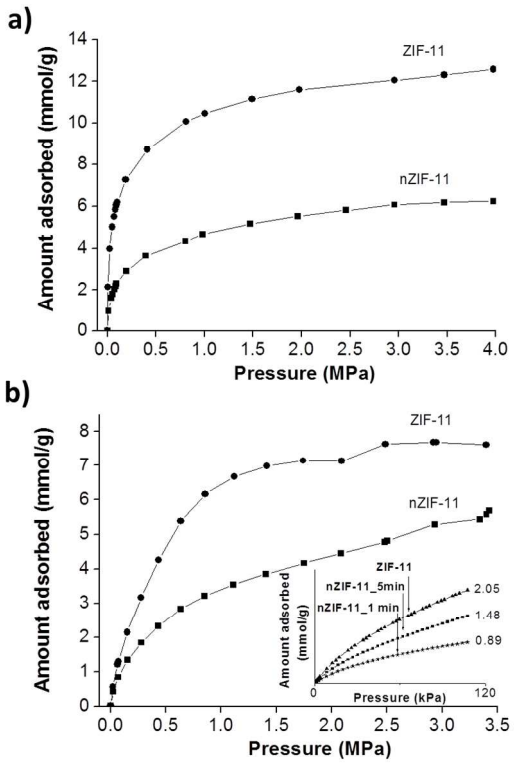

Figure 6. a) H_2 Excess adsorption isotherms at 77 K of micro- and nano-sized ZIF-11 from 0 to 40 bar and b) Absolute CO_2 adsorption isotherms for both samples at 273 K; Inset: CO_2 adsorption isotherm at 273 K from 0 to 120 kPa.

Fig. 6a shows a H_2 uptake of 6 mmol/g at 77 K and 4 MPa for nZIF-11, which is half of the amount adsorbed by the micro-sized MOF and found in the literature.[9] In Fig. 6b a CO_2 uptake of 5.9 mmol/g at 273 K and 3.4 MPa can be seen for nano-sized ZIF-11, which is approximately 30% smaller than the amount adsorbed by the micro-sized ZIF-11 sample under the same conditions. The Fig. 6b inset shows the low pressure CO_2 adsorption isotherms for both samples, together with the 1 min sample, where nZIF-11 depicts an intermediate sorption capacity. The micropore volume was calculated applying the Dubinin-Radushkevich equation to the low pressure region of the CO_2 absolute adsorption isotherms (up to 0.3 MPa).[29] The values obtained were 0.16 and 0.11 cm^3/g for micro- and nano-sized ZIF-11, respectively.

Under the experimental conditions studied, H_2 adsorption occurred in the microporous material[30] which explains the similar shape of both adsorption isotherms in Fig 6a. Then, the lower adsorption of H_2 in nZIF-11 compared to the micro-sized ZIF-11 indicates the lower amount of micropores in the former. However, CO_2 adsorption at 0 ^0C and up to 3.4 MPa (Fig. 6b) is sensitive to the whole range of porosity since the isotherm reaches a maximum relative fugacity close to 1.[29] The wider knee of the high pressure CO_2 isotherm for nZIF-11 suggests that this material has a wider pore size distribution and an amount of large pores, and a higher external surface. This may be a consequence of the difference in crystallinity of both materials, which may give rise to a broader pore

size distribution in the case of sample nZIF-11, contrary to its micro-sized counterpart which has a narrower knee in the CO_2 adsorption isotherm. Furthermore, as other authors have noted,[29] upon reaching pressures above around 2.5 MPa, CO_2 may condense in the mesoporosity (or intercrystalline space) of the samples. In this sense, the slope of the isotherm from this pressure and the upward curvature found in the last three adsorption data points found for the nano-sized sample is indicative of these wider pores, which once again may derive from the lower crystallinity of the sample.

It should be noted that CO_2 has been extensively reported in the literature as a suitable adsorbate for the characterization of narrow porosity (i.e. for pores of sizes around 3 Å, which correspond to the narrower cavities found for ZIF-11[9]) of adsorbents of markedly different chemical nature, not only carbon materials and carbon molecular sieves,[29] but also microporous crystalline inorganic oxides such as zeolites[31] and mesoporous materials such as MCM-41.[32] Thus, the results reported in this study serve to heighten the relevance of the crystallinity of ZIF-11 in the development of its porous texture.

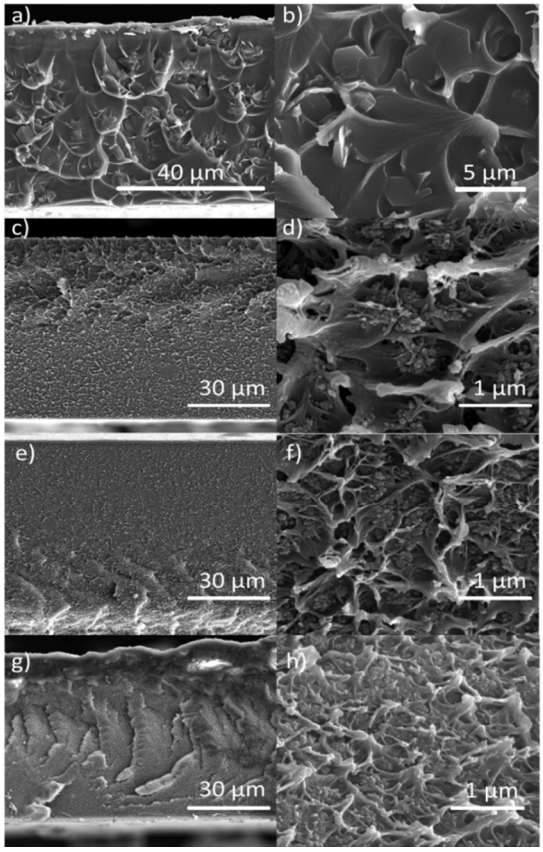

Figure 7. SEM images of Matrimid® MMMs 10 wt% loading with micro-sized ZIF-11 as filler (a, b) and 10wt% (c, d), 15 wt% (e, f) and 25 wt% (g, h) loading with nZIF-11_5min as filler.

Membrane characterization and performance

As a proof of application, ZIF-11 nanoparticles (specifically nZIF-11_5min) in both dried and wet conditions were integrated in the Matrimid® continuous phase in the form of MMMs. More stable, colloidal dispersions were obtained when nZIF-11 was processed in wet conditions without drying. In fact, Fig. S7 shows stability in chloroform for more than 20 days. The use of wet particles avoided agglomeration occurring when using the dried nanoparticles. Thus, MMMs comprising nominal loadings of 10, 15 and 25 wt% in dry basis of wet nZIF-11 (actual loadings tested by TGA being 9.1, 13.5 and 22.6 wt%, respectively) were prepared. The discrepancy between nominal and actual loadings comes from the use of the MOF in wet conditions without prior drying, only taking as reference the average yield calculated for the nZIF-11 synthesis.

The cross-sections of the membranes containing nominal loadings of 10, 15 and 25 wt% of nZIF-11 and 10 wt% micro-sized ZIF-11 (where large hexagonal ZIF-11 particles are evident) are shown in Fig 7. SEM images reveal the homogeneous dispersion and excellent adhesion of the filler particles within the polymeric phase.

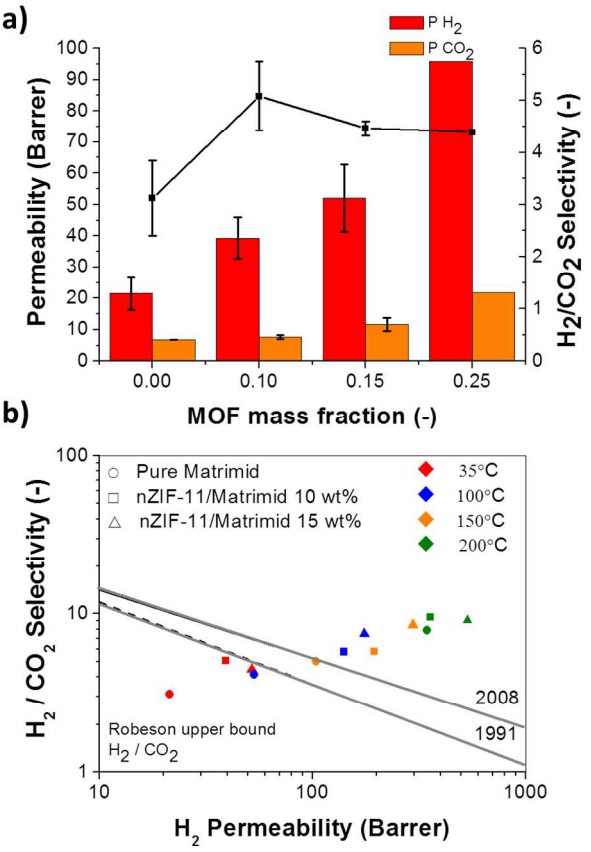

Figure 8. Gas separation performance of Matrimid® MMMs containing nZIF-11_5min at 35ºC (a) and as a function of the temperature (b).

Figure 8a shows the H_2/CO_2 gas separation performance for a 50/50 mixture at 35 ºC and 2 bar of driving force. At least 2-3 MMMs of each loading were fabricated and measured, except for the 25 wt% loading, to provide error estimations. The integration of nZIF-11 in membranes enhanced the permeability for both gases, achieving a higher selectivity in comparison with the pure polymer. However, while permeability continuously increased as a function of the membrane loading, selectivity decreased for the 15 wt% MMMs and then maintained constant. This suggests the presence of non-selective voids owing to some deterioration in the interaction

between MOF and polymer at these high loadings.[33] This oscillating behavior has also been reported in the literature for Matrimid® MMMs comprising ZIF-8.[34] These results are also in good agreement with the single published paper reporting micro-sized ZIF-11 in the form of MMMs.[35] In this case ZIF-11 was embedded in PBI polymer giving rise to an improvement in permeability when increasing the loading (PH_2= 17.2 Barrer for pure polymer membrane to 67.8 Barrer for 16.1 wt% loading and 133.1 Barrer for 29.7 wt%) but the selectivity barely improved over the pure polymer ($\alpha H_2/CO_2$=5.0 for PBI, 5.6 for 16.1 wt% loading and 3.7 for 29.7 wt%).

In addition, 10 wt% nZIF-11 MMMs produced higher H_2 permeability and H_2/CO_2 selectivity (44.5 Barrer and 5.6, respectively) than the corresponding MMMs with micro-sized ZIF-11 (38.3 Barrer and 4.8, respectively). In any event, the highest loading membrane (25 wt%) produced 95.9 Barrer of H_2 with a H_2/CO_2 selectivity of 4.4.

Thus, in order to improve the membrane performance, experiments at high temperature (35-200 ºC range) were carried out with 10 and 15 wt% MMMs (**Figure 8b**). Matrimid® has a high thermal stability with a glass transition temperature of about 320 ºC.[36] Raising the temperature has a beneficial effect on the separation performance, surpassing the Robeson upper bond[37] over 100 ºC. Although only the Robeson upper bound at 35^{0}C is represented, it only shifts upwards slightly with increasing temperature[38] and the measured values would continue being over it. In any event, permselectivity results of nZIF-11 MMMs at each temperature are always higher than the bare polymer membrane. As expected, the permeability increased due to a higher diffusion of the penetrants, while CO_2 adsorption on the MOF and solution in the polymer decreased. All membranes showed permeation at least 300 Barrer higher at 200 ºC than at 35 ºC. Selectivity also increased with temperature, duplicating its value from the lowest to the highest temperature for each membrane. The best result obtained with 15 wt% loading of nZIF-11 corresponds to 535 Barrer of H_2 with a H_2/CO_2 selectivity of 9.1. A comparison with other MMMs containing ZIFs found in the literature regarding this mixture is included as supporting information (Table S2).

Even though high selectivity values are expected due to the small pore apertures of ZIF-11 (3.0 Å) and the molecular size of both molecules of H_2 (2.9 Å) and CO_2 (3.3 Å), the flexibility of the ZIFs plays an important role leading to lower values than predicted as suggested by Bux et al.[39]

Apparent activation energy was calculated for H_2, the fastest permeating compound in the binary mixture, resulting in values of 14.7 kJ/mol for the pure polymer and 15.7 and 16.8 kJ/mol for the 10 wt% and 15 wt% loaded MMMs, respectively. This increase in the activation energy as a function of the filler loading suggests the positive influence of the ZIF microporosity on the transport properties of the membrane. Activated transport in the case of H_2/CO_2 has recently been found when testing MMMs comprising polysulfone and the filler MSS-Z8 (silica-ZIF-8 core shell spheres with ordered meso-microporosity) with 32 wt% loading at high temperature (120 ^{0}C), giving rise to higher H_2 permeabilities with similar selectivities.[40]

Conclusions

Nano-sized MOF ZIF-11 (nZIF-11) has been synthesized through a new technique based on centrifugaminecol acceleration for obtaining nanoparticles. This technique makes possible the synthesis and separation of the MOF material in only one step. From the characterization carried out, the nanoparticles (36±6 nm) showed the same thermal stability, similar bond structure in terms of both FTIR and NMR and analogous H_2 and CO_2 adsorption capacities as the micrometric particles.

Due to their smaller size, they were easily integrated with high loading (10-25 wt%) in a polymeric continuous phase to produce mixed matrix membranes. It was necessary to keep the filler in a wet state to avoid agglomeration. Mixed matrix membranes containing nZIF-11 displayed a high performance for H_2/CO_2 separation, which improved at high temperatures due to the simultaneous increase in both permeability (because of H_2 activated diffusion) and H_2/CO_2 selectivity (because of the decreasing CO_2 adsorption and solution).

Acknowledgements

Financial support from the Spanish MINECO (MAT2013-40566-R, CTQ2012-31762, and RyC-2009-03913), the Aragón Government and the ESF is gratefully acknowledged. In addition, the research leading to these results has received funding from the European Union Seventh Framework Programme (FP7/2007-2013) under grant agreement n° 608490, project M4CO2. Finally, the use of the Servicio General de Apoyo a la Investigación-SAI (Universidad de Zaragoza) is acknowledged.

Notes and references

[1]Chemical and Environmental Engineering Department and Instituto de Nanociencia de Aragón (INA), Universidad de Zaragoza, 50018 Zaragoza, Spain

[2]Laboratorio de Microscopías Avanzadas (LMA), Nanoscience Institute of Aragón (INA), Universidad de Zaragoza, 50018 Zaragoza. Spain

[3]Alicante Materials Institute and Inorganic Chemistry Department, University of Alicante, 03080 Alicante. Spain

1 Y. Lee, J. Kim and W. Ahn, *Korean J. Chem. Eng.,* 2013, **30,** 1667-1680.
2 G. Ferey and C. Serre, *Chem. Soc. Rev.,* 2009, **38,** 1380-1399.
3 B. Zornoza, C. Tellez, J. Coronas, J. Gascon and F. Kapteijn, *Microporous Mesoporous Mater.,* 2013, **166,** 67-78.
4 H. B. T. Jeazet, C. Staudt and C. Janiak, *Dalton Trans.,* 2012, **41,** 14003-14027.
5 P. Horcajada, C. Serre, M. Vallet-Regí, M. Sebban, F. Taulelle and G. Férey, *Angew. Chem. Int. Ed,* 2006, **118,** 6120-6124.
6 H. Jiang, T. Akita, T. Ishida, M. Haruta and Q. Xu, *J. Am. Chem. Soc.,* 2011, **133,** 1304-1306.
7 J. Gascon, U. Aktay, M. D. Hernandez-Alonso, G. P. M. van Klink and F. Kapteijn, *J. Catal.,* 2009, **261,** 75-87.
8 J. C. Tan, T. D. Bennett and A. K. Cheetham, *Proc. Natl. Acad. Sci. U. S. A.,* 2010, **107,** 9938-9943.
9 K. S. Park, Z. N. Ni, A. P. Coˆ te, J. Y. Choi, R. Huang, F. J. Uribe-Romo, H. K. Chae, M. O'Keeffe and O. M. Yaghi, *PNAS,* 2006, **103,** 10186-10191.
10 A. W. Thornton, D. Dubbeldam, M. S. Liu, B. P. Ladewig, A. J. Hilla and M. R. Hill, *Energy Environ. Sci.,* 2012, **5,** 7637–7646.

11 S. K. Nune, P. K. Thallapally, A. Dohnalkova, C. Wang, J. Liu and G. J. Exarhos, *Chem. Commun.,* 2010, **46,** 4878-4880.
12 J. Cravillon, S. Muenzer, S. Lohmeier, A. Feldhoff, K. Huber and M. Wiebcke, *Chem. Mater.,* 2009, **21,** 1410-1412.
13 L. Qiu, Z. Li, Y. Wu, W. Wang, T. Xu and X. Jiang, *Chem. Commun.,* 2008, 3642-3644.
14 B. Zornoza, A. Martinez-Joaristi, P. Serra-Crespo, C. Tellez, J. Coronas, J. Gascon and F. Kapteijn, *Chem. Commun.,* 2011, **47,** 9522-9524.
15 D. Tanaka, A. Henke, K. Albrecht, M. Moeller, K. Nakagawa, S. Kitagawa and J. Groll, *Nat. Chem.,* 2010, **2,** 410-416.
16 L. Paseta, B. Seoane, D. Julve, V. Sebastian, C. Tellez and J. Coronas, *Acs Appl. Mater. Interfaces,* 2013, **5,** 9405-9410.
17 Minh-Hao Pham, Gia-Thanh Vuong, Anh-Tuan Vu and Trong-On Do, *Langmuir,* 2011, **27,** 15261-15267.
18 Y.-S. Li, F.-Y. Liang, H. Bux, A. Feldhoff, W.-S. Yang, J. Caro, *Andgew. Chem. Int. Ed.,* 2010, 548–551.
19 Y. Pan, Y. Liu, G. Zeng, L. Zhao and Z. Lai, *Chem. Commun.,* 2011, **47,** 2071-2073.
20 W. Morris, N. He, K. G. Ray, P. Klonowski, F. Hiroyasu, I. N. Daniels, Y. A. Houndonougbo, M. Asta, O. M. Yaghi and B. B. Laird, *J. Phys. Chem.,* 2012, **116,** 24084–24090.
21 M. He, J. Yao, Q. Liu, Z. Zhongb and H. Wang, *Dalton Trans.,* 2013, **42,** 16608-16608–16613.
22 A. Corma and M. J. Diaz-Cabanas, *Microporous Mesoporous Mater.,* 2006, **89,** 39-46.
23 J. Gascon, S. Aguado and F. Kapteijn, *Microporous Mesoporous Mater.,* 2008, **113,** 132-138.
24 S. Surble, F. Millange, C. Serre, G. Ferey and R. I. Walton, *Chem. Commun.,* 2006, 1518-1520.
25 T. Yang, Y. Xiao and T. Chung, *Energy Environmental Sci.,* 2011, **4,** 4171-4180.
26 C. Zhang, X. S. Lu and A. Z. Gu, *Int. J. Hydrogen Energy,* 2004, **29,** 1271-1276.
27 T. Kiyobayashi, H. T. Takeshita, H. Tanaka, N. Takeichi, A. Zuttel, L. Schlapbach and N. Kuriyama, *J. Alloys Compounds,* 2002, **330,** 666-669.
28 R. F. Egerton, P. Li and M. Malac, *Micron,* 2004, **35,** 399-409.
29 D. Cazorla-Amoros, J. Alcaniz-Monge, M. A. de la Casa-Lillo and A. Linares-Solano, *Langmuir,* 1998, **14,** 4589-4596.
30 M. Jorda-Beneyto, F. Suarez-Garcia, D. Lozano-Castello, D. Cazorla-Amoros and A. Linares-Solano, *Carbon,* 2007, **45,** 293-303.
31 J. Garcia-Martinez, D. Cazorla-Amoros and A. Linares-Solano, *Stud. Surf. Sci. Catal.,* 2000, **128,** 485-494.
32 Á. Berenguer-Murcia, D. Cazorla-Amorós and Á. Linares-Solano, *Adsorpt. Sci.,* 2011, **29,** 443-455.
33 R. Mahajan, R. Burns, M. Schaeffer and W. J. Koros, *J Appl Polym Sci,* 2002, **86,** 881-890.
34 M. J. C. Ordonez, K. J. Balkus Jr., J. P. Ferraris and I. H. Musselman, *J. Membr. Sci.,* 2010, **361,** 28-37.
35 L. Li, Y. Jianfeng, X. Wang, Y. Chen and H. Wang, *J. Appl. Polym. Sci.,* 2014, **131,** 41056.
36 B. Zornoza, C. Téllez and J. Coronas, *J. Membr. Sci.,* 2011, **368,** 100-109.
37 L. M. Robeson, *J. Membr. Sci.,* 2008, **320,** 390-400.
38 B. W. Rowe, L. M. Robeson, B. D. Freeman and D. R. Paul, *J. Membr. Sci.,* 2010, **360,** 58-69.
39 H. Bux, F. Liang, Y. Li, J. Cravillon, M. Wiebcke and J. Caro, *J. Am. Chem. Soc.,* 2009, **131,** 16000-16001.
40 S. Sorribas, B. Zornoza, C. Téllez and J. Coronas, *J. Membr. Sci.,* 2014, **452,** 184-192.

Graphical abstract and contents text

Beyond the H_2/CO_2 upper bound: one-step crystallization and separation of nano-sized ZIF-11 by centrifugation and its application in mixed matrix membranes

Javier Sánchez-Laínez, Beatriz Zornoza, Álvaro Mayoral, Ángel Berenguer-Murcia, Diego Cazorla-Amorós, Carlos Téllez, Joaquín Coronas,*

Nano-sized ZIF-11 with an average size of 36±6 nm and similar features to ZIF-11 has been applied to the adsorption of H_2 and CO_2 and to the preparation of mixed matrix membranes for H_2/CO_2 separation.